Preparation, Characterisation and Electrochromic Property of Mesostructured Tungsten Oxide Films via a Surfactant Templated Sol-Gel Process from Tungstic acid

Wei Wang [A] Yongxin Pang [A] Simon N. B. Hodgson [A,B]
[A] School of Science and Technology, University of Teesside, UK
[B] Email: s.n.hodgson@tees.ac.uk

Abstract

A novel kind of mesoporous tungsten oxide films (TOFs) has been prepared via a non-ionic surfactant templated sol-gel route from cheap and easy handling tungstic acid. Characterisations by means of various techniques, including XRD, TEM, SEM, ATR and DTA, confirm that the obtained mesostructures are composed of fine mesopores (2-3nm) and thin pore walls. Compared with previously reported surfactant templated mesoporous TOFs, our initial evaluation on the electrochromic properties showed that the derived TOFs show greatly enhanced colouration efficiency of 44cm^{2}C^{-1} and faster colouration/bleaching speed of 10/2 seconds, respectively. Owning to the ordering of mesostructures delivered by our method, the mesostructural changes associated with the electrochemical reaction during the electrochromic cycling of such materials can be directly monitored by low-angle XRD measurements.

Keywords: mesoporous, tungsten oxide film, sol-gel, electrochromism,.

1. Introduction

Over recent years, electrochromism has received substantial attention for smart applications, such as self-dimming rear-view mirrors, sun-protective windows and optical displays [1]. Compared with conducting polymer systems (e.g. polythiophene, polypyrrole), WO_3 is often regarded as a more promising candidate material, due to its transparency and good reversibility in colour change when an external electrical field is applied [2, 3] and is the most widely used and most cited cathodically-colouring material in the patent literature. Various methods have been developed to synthesise tungsten oxide films (TOFs), including laser ablation [4], anodic oxidation [5], sputtering [6], and electrodeposition [7]. Compared with these methods, sol–gel processing is an inexpensive, simple and controllable alternative, facilitating the bespoke engineering of a variety of nanostructures. For example, mesoporous materials with high surface area can be obtained by surfactant templated sol-gel process [8, 9]. Via this synthetic route, a number of metal oxides, including WO_3, have been synthesised [10].

It has been previously reported in studies of materials produced by other routes that mesostructured TOFs, allow rapid ion transport through the bulk of the film, and hence improve colouration efficiency and colour–bleach kinetics [11]. Deepa and co-workers also reported that the fast colour-bleach kinetics in mesostructured TOFs were associated with the mesopore morphology [12]. Cheng and co-workers demonstrated that mesoporous structures generated by a block copolymer templated sol-gel

method using WCl_6 as precursor exhibited better kinetics for colouration and bleaching in comparison to the normal sol–gel-derived TOFs. Upon colouration at -0.8V (vs SCE) for 30s, the transmission is higher than 30% for mesostructured TOFs with thickness over 400nm [13], suggesting the electrochromic efficiency is low. In general, high manufacturing costs and unsatisfactory electrochromic durability have been obstacles for the applicability of electrochromism. Current challenges include further accelerating the coloration/bleaching process, enhancement of the charge density and especially the reduction in manufacturing cost of TOFs. Therefore, there is a requirement for further improvements in the electrochromic properties and fabrication process as well in order to allow them to be commercially developed.

In the chemical preparation of mesoporous tungsten oxide, WCl_6 is the most often selected inorganic precursor [14]. Alternatively, tungstic acid which is comparatively cheap and easily handled has also been used as an alternative precursor to prepare nonporous sol-gel WO_3 films for various applications [3, 10, 15]. However, tungstic acid has only received very limited investigation as a potential precursor for the preparation of mesostructured TOFs. Work by Qi and co-workers [16] attempted to prepare mesostructured TOFs by utilising block copolymer as structure-directing agent and tungstic acid as tungsten oxide precursor. However, the resulting mesostructures collapsed upon heating at temperatures higher than 250 ^{o}C. Improvement in the thermal stability is of some significance for the development of viable mesostructured TOF's from this precursor, as a heat treatment to at least this temperature is required to facilitate consolidation of the film and give good adhesion to the substrate, whilst higher temperatures are required to thermally remove the organic surfactant to create an accessible mesopore structure.

Recently, our research group has demonstrated the feasibility of fabricating thermally stable mesoporous TOFs from cheap tungstic acid [17]. In this paper, detailed characterisation of the mesostructures and the resultant properties, especially the electrochromic properties of the derived TOFs are discussed, aiming to demonstrate a new, cheap, easy and reliable surfactant templated sol-gel method for the fabrication of mesostructured TOFs with great potential in electrochromic devices.

2. Experimental details

The following chemicals were used in the preparation of the TOFs. Tungstic acid (≥99.0%) obtained from Fluka, H_2O_2 35wt.% water solution and the non-ionic surfactants Brij56 ($C_{16}EO_{10}$, $C_{16}H_{33}(OCH_2CH_2)_nOH$, n~10), Tween-60 ($C_{24}H_{46}O_6(C_2H_4O)_n$, n~20) were obtained from Sigma Aldrich. All the chemicals were used as received.

Peroxotungstic acid (PTA) was synthesized through the reaction of H_2WO_4 with hydrogen peroxide. Typically, 5.0 g of H_2WO_4 powders were dispersed in 100.0 g of deionised water, to which 33.0 g H_2O_2 35 wt.% aqueous solution was added. The reaction mixture was magnetically stirred at 40 ^{o}C overnight to produce a nearly colourless solution and then dried to produce the pale yellow PTA powder. The coating sol was prepared by mixing the solutions of PTA and surfactant in mixed solvents of water and ethanol, with a final weight ratio of PTA: Surfactant: H_2O: Ethanol of 1: 0.2: 4.5: 2.25. The sol was used for dip-coating on cleaned glass substrates or Indium-Tin oxide (ITO) coated glasses under ambient conditions. The deposited film was allowed to dry at room temperature and then, was further

thermally treated at temperatures at 100-450 ^{o}C for between 1-20 h to solidify the film and remove the template.

X-ray Diffraction (XRD) measurement was conducted on a Siemens D500/D501 instrument with CuK_{α} radiation (λ=0.1542 nm) at a scanning speed of 0.01 ^{o} per second, using low angle diffraction peaks to determine the interpore distances according to the normal Bragg relationship. Accurate estimation of the pore spacing requires the mesostructures to be highly ordered with known geometry. As this could not be confirmed in this case, such results should be considered to provide only an approximation of the mesostructural scale, assuming mesopores are hexagonally arranged analogous to MCM-41 [8-9]. Transmission electron microscopy was performed using a Philips CM100 instrument operated at 100 kV. Samples for transmission electron microscope (TEM) measurement were obtained by scratching off the heat treated film coating from the glass substrates, this being then dispersed in acetone and mounted on copper grids. Attenuated total reflectance spectra of powder samples obtained by drying coating sols were collected using a Nicolet 5700 FTIR spectrometer.

The electrochemical properties were determined using a three electrode configuration in which the working electrode consisted of the dip coated TOFs deposited on ITO coated glass in 0.1 M aqueous solution of sulphuric acid. An Ag electrode (Ag|AgCl|saturated KCl) and a platinum needle were taken as the reference and counter electrode, respectively. The voltammetry and chronoamperometry experiments were performed using an Autolab 12 potentiostat with GPES software for collection and analysis of data. The optical spectra were collected using a Jasco V-630/630BIO UV-Vis spectrophotometer with scanning speed of 200 nm/min.

3. Results and discussion

3.1 Morphological and structural studies of PTA/surfactant hybrid film

Non-ionic surfactants, such as Brij 56 and Tween 60, which have previously been used for the synthesis of (MSU-X) mesoporous silicas [18, 19], were employed in this work. In the templating systems for mesoporous silicas, interactions between silicate species with the poly(ethylene glycol) (PEG) segments in surfactant molecules via hydrogen-bonding promote the self-assembly process, which is responsible for the formation of mesophases. A similar mechanism is anticipated to produce the templating in the preparation of the TOF's, but with the PTA species substituting for the silicates.

It has been proposed that, aside from their function as structure-directing agents, the ethylene glycol (EG) segments in the nonionic surfactant molecules are incorporated into the oxide framework walls by complexing with PTA species and, hence have a strong influence on the flexibility and thermal stability of the obtained TOFs mesostructures. In comparison with some other ineffective organic surfactant templated systems tested in our previous work [17], Tween 60 showed no improvement in templating the formation of mesoporous TOFs according to the XRD results (Fig.1(c-d)). This is again in big contrast with the Brij 56 templated TOFs.

A weight ratio of PTA to Brij 56 of 5 (m(PTA): m(Brij 56)=5) was found to yield the most thermally stable and ordered mesostructures. This paper is therefore focused on these optimised Brij 56 templated TOFs with PTA: Brij 56 weight ratio fixed at 5:1. Fig. 1a-b show XRD patterns obtained from the

as-prepared TOFs using Brij 56 ($C_{16}EO_{10}$) as the template. The resultant TOFs show a strong peak centred at about 1.5°, corresponding to a d-spacing of about 5.9 nm (Fig. 1(a)). This is very similar to the values reported for mesoporous silicas using the same template, implying that a similar templating mechanism applies for both PTA anions and silica anions in association with the same organic template [19]. For the film dried at 100 °C for 1 h (Fig. 1(b)), the calculated d-spacing is about 4.4 nm (2θ value is about 2 °) and only one strong peak can be seen, indexed as (100) in hexagonal mesophase. Fig. 2 shows the TEM images for the PTA/Brij 56 hybrid films, heated at temperatures ranging from 100 °C to 400 °C, which provide direct evidences of the hexagonally ordered mesostructures. As can be seen from Fig. 2(a) ordered mesostructures to a great extent are present with mesopore (still occupied by organic template in this stage) size of 3.5 nm.

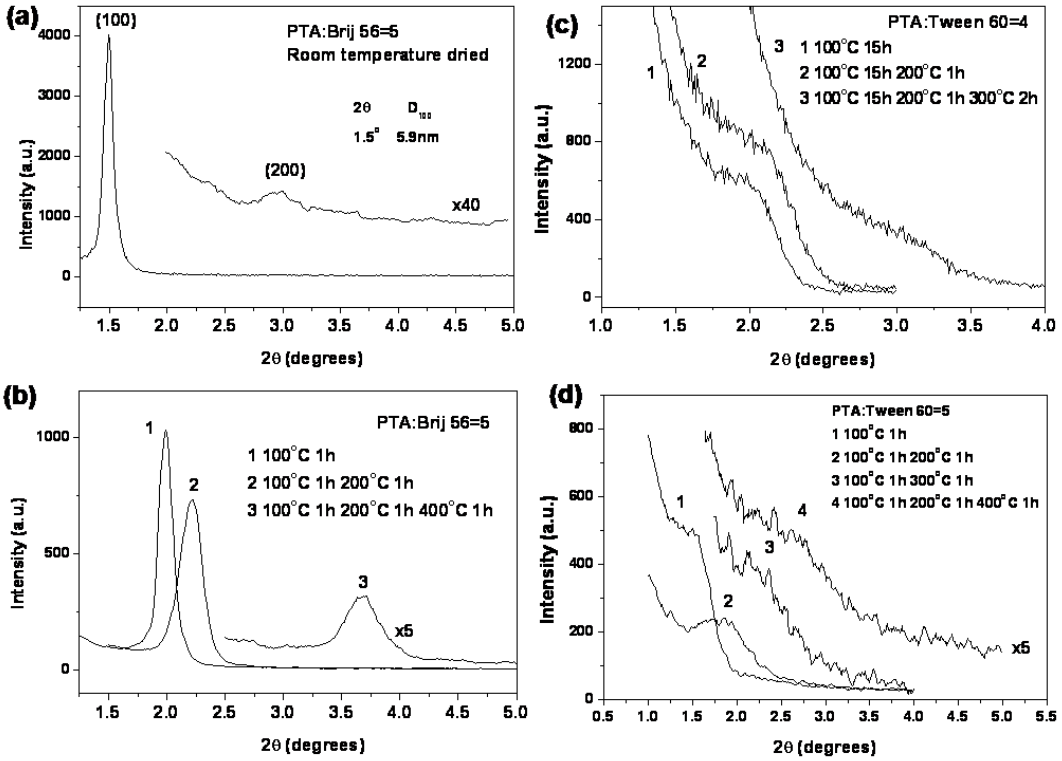

Fig. 1 XRD patterns of PTA/Brij 56 films (m(PTA): m(Brij 56)=5), (a)dried at room temperature, and (b) heated at different temperatures; and XRD patterns of PTA/Brij Tween 60 films with (c) (m(PTA): m(Tween 60) of 4 and(d) (m(PTA): m(Tween 60) of 5.

Heat treatment at higher temperatures (e.g. 200 °C as shown in Fig. 1(b), pattern 2) and 250 °C (XRD not shown here) did not damage the mesostructures, which was confirmed by TEM results (190 °C, Fig. 2(b), and 250 °C, Fig. 2(c)), whilst even after heating to 400 °C for 2 h, the low angle XRD peak is still observable, though broadened from about 0.13 ° to 0.33 ° in full width at half maximum (FWHM), indicating the retention of mesostructures. This was confirmed by TEM results (Fig. 2(d)) in which the mesostructures with pore size of approximately 2 nm and wall thickness around 1 nm can be discerned, although the ordering of the mesostructure is degraded. TEM images further showed that mesopores are all open from above and therefore accessible at the surface, which is believed to be advantageous in electrochromism in terms of increased electrolyte accessible surface area and shortened diffusion time as well.

Among the few mesostructured TOFs prepared by surfactant templated sol-gel method [13, 14d-f], the pore size and wall thickness of mesostructured TOFs reported in this work are shown to be lowest, and hence the surface area is theoretically the highest. The thickness of our mesostructured TOFs is about 200 nm on average and crack-free as measured using SEM and optical microscope (results not shown here). Such thin film makes it hard to quantify the surface area by using N_2 sorption measurement. The surface area of mesostructured TOFs was estimated to be up to 250m^2/g based on surface areas of silicas with similar mesostructures and the densities (d(SiO_2) = 2.2 g/cm^3, (d(WO3) = 7.16 g/cm^3) [19] .

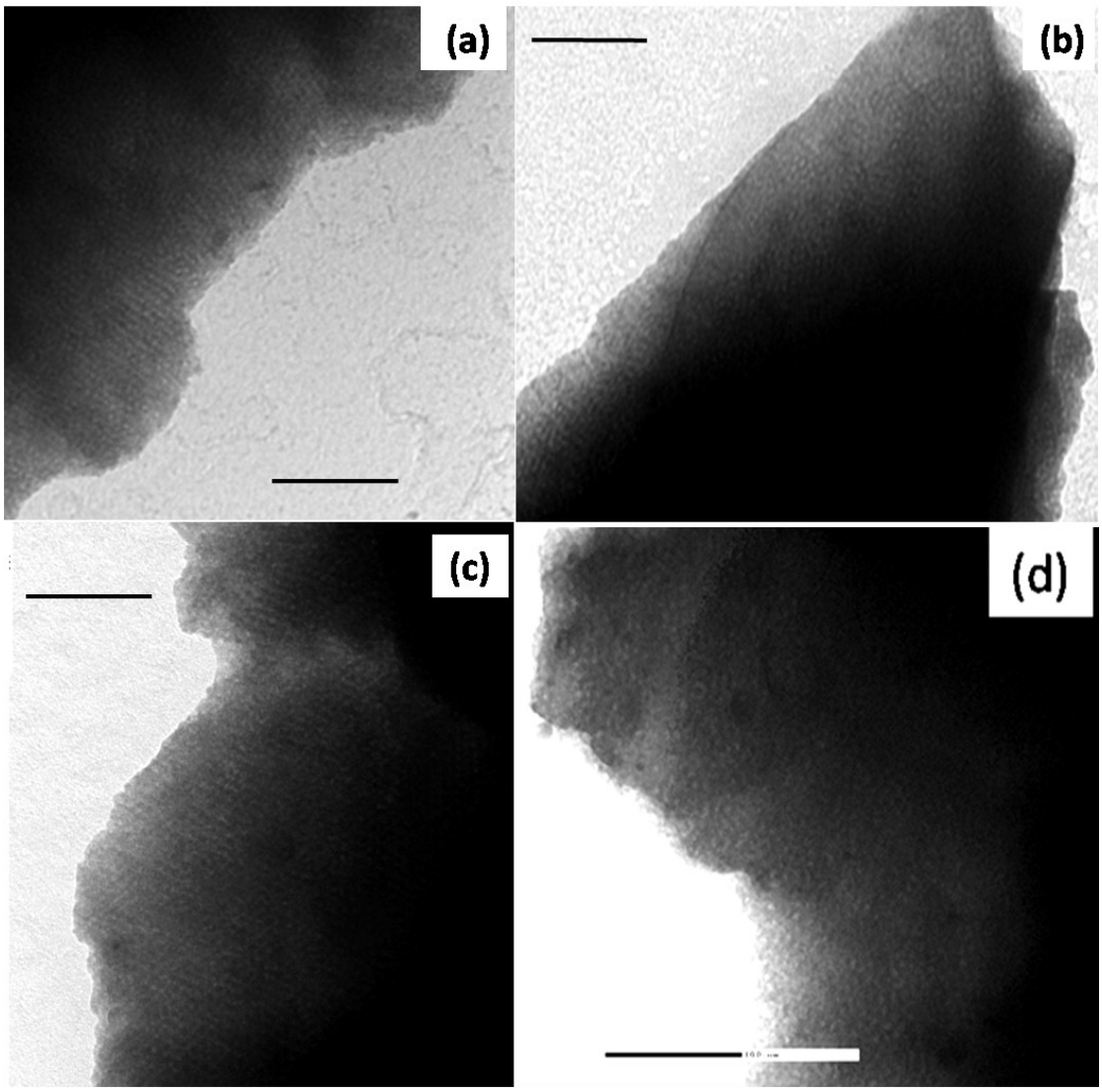

Fig. 2 TEM images of TOFs (m(PTA): m(Brij 56)=5) heated at (a) 100 ^oC, 1 h, (b) 100 ^oC,1 h+190 ^oC,1 h, (c) 250 ^oC, 2 h, and (d) 250 ^oC, 2 h + 400 ^oC, 2 h. Scale bars=100 nm.

One of the main characteristics of the obtained mesostructures of Brij 56-templated PTA film is the substantial 2θ shift in low-angle XRD peaks upon heat treatment, as shown in Fig. 1. This not only differs from the behaviour of similarly templated silicate structures [18,19], but also contrasts with the previously reported behaviour of surfactant templated WCl_6 derived sol-gel mesostructured films, where no significant shift in low-angle XRD peak was observed after heat treatment [20]. The probable reason lies in the hydrolysis and condensation of WCl_6 in the presence of water taking place at different stages during the structure development, which allowed the improvement in cross-linking reaction

between tungsten oxide species and consolidation of the film such that it becomes strong and rigid enough to withstand heating at elevated temperatures. By contrast, PTA species derived framework contains significant amounts of structural water and peroxo tungsten oxide species and would therefore be expected to undergo much bigger changes upon heat treatment than WCl_6 derived tungsten oxide species.

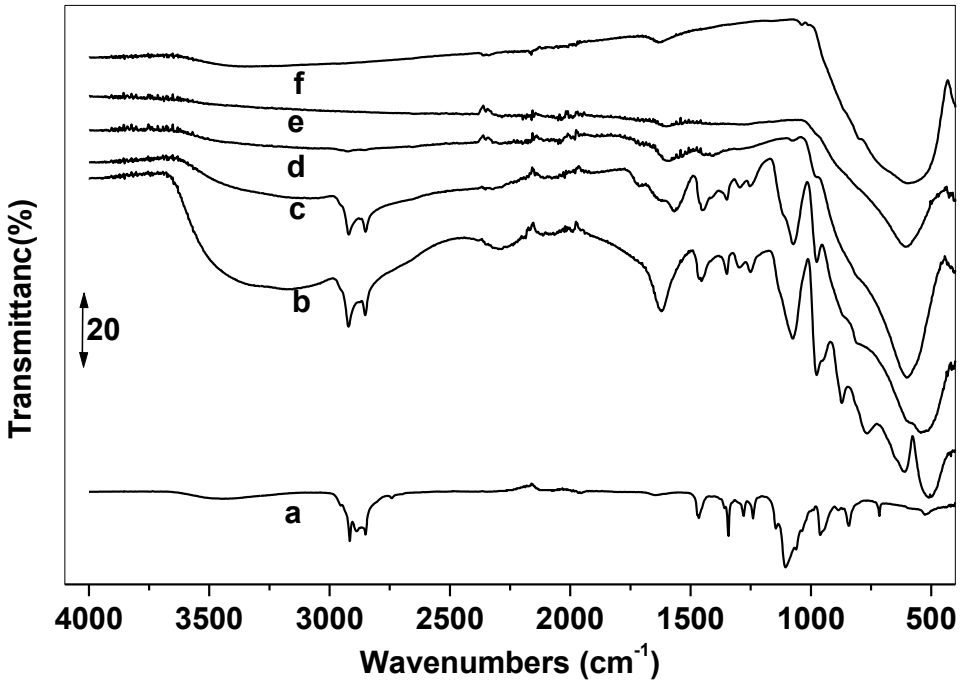

Fig. 3 Attenuated total reflectance of (a) Pure Brij 56, and (b-f) PTA/Brij 56 hybrids (m(PTA): m(Brij 56)=5) after various heat treatments (b) as prepared, (c) 100 ^{o}C for 1 h, (d) 100^{o}C+190^{o}C for 1h, (e) 100^{o}C+250 ^{o}C for 1 h, and (f) 190 ^{o}C for 1 h and then 400 ^{o}C for 1 h.

In the case of the Brij 56 templated PTA system, the optimisation of heating process was also found to be crucial to generate thermally stable mesoporous tungsten oxides. An additional heat treatment step at intermediate temperatures, such as 190 ^{o}C or 250 ^{o}C, was found to effectively stabilise the frameworks allowing them to sustain further heat treatment at high temperatures up to 450 ^{o}C [17]. In order to further clarify the reactions occurring in the PTA/Brij 56 hybrid films during the heat treatments, attenuated total reflectance spectra were collected on samples heated at varying temperatures (Fig. 3).

In samples heat treated at temperatures below 200 ^{o}C, absorption band at 1620 cm^{-1}, which can be assigned to water, is present, with its intensity decreasing with increasing heat treatment temperature. In addition, absorption bands attributable to the organic groups of Brij 56 molecules are identifiable in the PTA/Brij 56 hybrids, with decreasing intensity in samples heated to increasing temperatures up to 250 ^{o}C, confirming the gradual decomposition of the surfactant. These absorption bands comprise C-H stretching absorption at 2925 and 2849 cm^{-1}, different -CH_2- bend, wag, rock, and twisting modes at 1250-1450 cm^{-1}, with the comparatively stronger band at 1077 cm^{-1} due to C-O-C stretching [20]. As can be seen from Fig. 3(d-f), the decomposition of organic structure and the low residual levels explain the lack of identifiable ATR peaks for TOFs heated at temperatures over 250^{o}C.

Additionally, one intense band at around 520 cm^{-1}, which can be attributed to the stretching vibration of $W(O_2)$ groups [21] is present in those samples subjected to heat treatment at 100 ^oC for 1 h but is not present in the sample heated at 190 ^oC for a similar duration. This correlates with thermal analysis results (results not shown here) and can be attributed to the decomposition of peroxo groups at temperatures higher than 130 ^oC. For all the samples (Fig. 3(b-f)), a very broad band at around 620 cm^{-1} due to the stretching vibration of W–O–W linkage is always present and increases in intensity with heating temperature (Fig. 3(d) and (e)), indicating that the heating treatment at 190 and 250 ^oC promotes condensation reaction of the tungsten oxide species. Again, this is in good correlation with the results of thermal analysis and explains why heat treatment at intermediate temperatures is important for preparing thermally stable mesostructural TOFs.

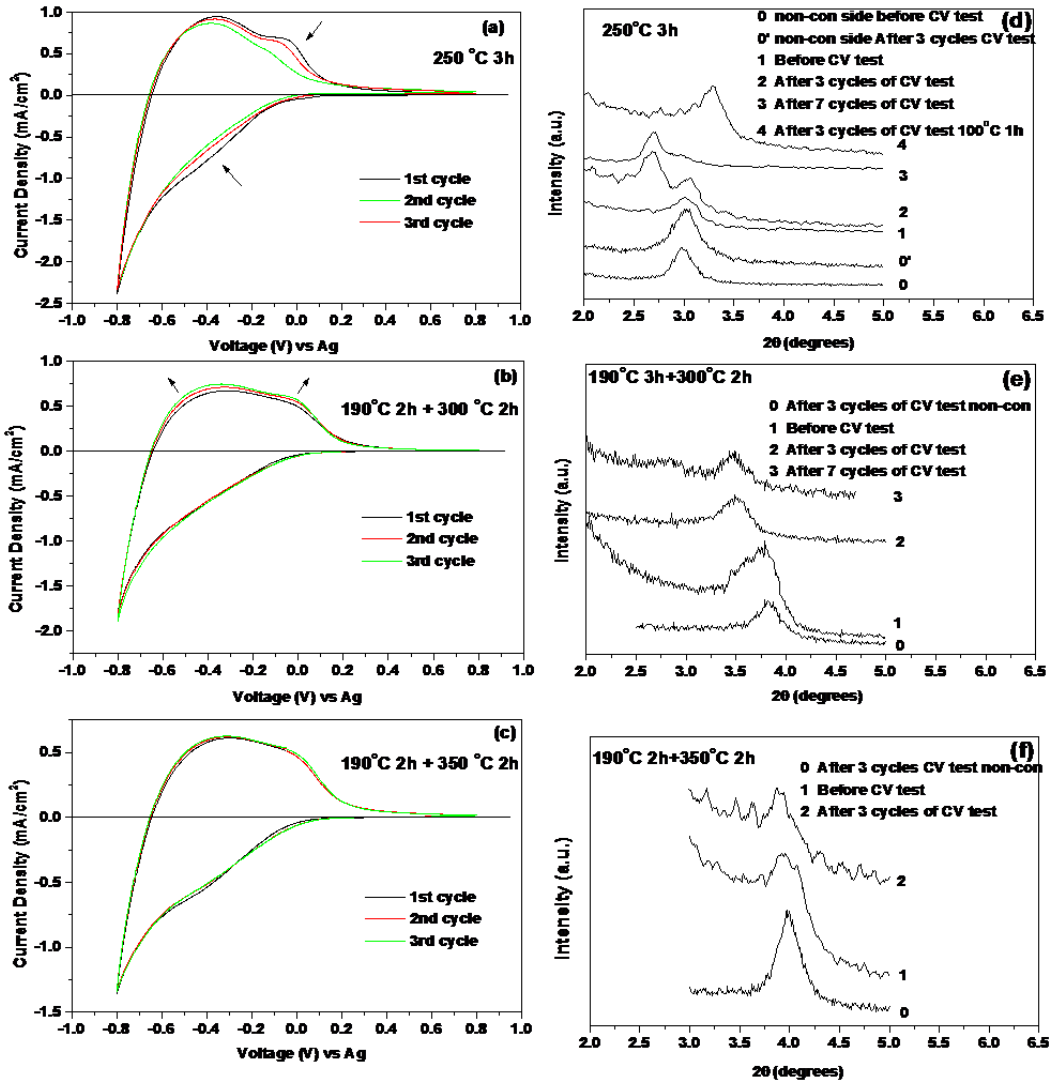

Fig. 4 Cyclic voltammograms (a-c) and XRD patterns (d-f) of mesostructured TOFs coated on ITO glass after heating at (a & d) 250 ^oC for 3 h, (b & e) 190 ^oC 2 h+300 ^oC 2 h, (c & f)190 ^oC 2 h+350 ^oC 2 h. The voltage alternated between 0.8 V and -0.8 V vs Ag electrode and the sweep rate was set to be 10 mVs^{-1}. An inclusion of the XRD patterns of TOFs coated on the non-conductive side of ITO coated glass is for comparison use. In the XRD patterns, those designated as zero represent the TOFs on the non-conductive sides of ITO glass (designated as non-con in the figure) whilst all the other patterns are

obtained from the TOFs coated on the conductive sides. Arrows in figure a-c indicate the evolution of cyclic voltammograms during 3 cycles. Some XRD patterns were shifted to avoid overlap.

3.2 Cyclic voltammetry (CV) studies of mesostructured TOFs

In order to examine the electrochromic properties the mesostructured TOFs were coated on ITO coated glass for the cyclic voltammetry measurements. The colouration process of the electrochromic films can be described as a function of simultaneous injection of protons and electrons inside the mesoporous WO_3 framework walls as shown in Eq.(1).

$$WO_3(colourless) + xH^+ + xe^- \leftrightarrow H_xWO_3(blue) \qquad \text{(Eq.1)}$$

Fig. 4(a-c) show the cyclic voltammograms of mesostructured WO_3 thin films coated on the ITO (conductive) side of ITO glass heated at varying temperatures and times. Fig. 4(d-f) show the corresponding XRD patterns for the mesoporous TOFs heated at different temperatures before (pattern 1) and after (patterns 2, 3, 4) CV testing. As can be seen from pattern 1 in each of these figures, the XRD results for TOFs before CV testing are consistent with above XRD results discussed in section 3.1, regarding the effects of heat treatment, i.e. heat treatment at higher temperature led to the reduction and broadening of the XRD low angle peak but with the mesostructures being retained.

It can be seen that the mesostructured TOFs exhibited well-defined main anodic peaks at about -0.37 V for all three samples studied here (Fig. 4(a-c)). No significant residual current (current at end of the anodic scan [14f]) was found after each cycle for all three samples, indicating that extraction process for protons can be completed at the end of the anodic scan at 0.8 V or less. However, with respect to the electrochemical reversibility, an obvious dependence on the heat treatment temperature of the films can be observed; the 350 ^oC heated film (Fig. 4c) is the best among them, its voltammograms nearly completely overlapping with each other during three cycles.

Table 1 Electrochemical characteristics of Brij56 template TOFs heated at different temperatures as shown in Fig. 4(a-c) .

Sample	cycles	Anodic peak/V vs Ag	Amount of charge inserted Q^-/mCcm^{-2}	Amount of charge extracted Q^+/mCcm^{-2}	Q^+/Q^-
250 ^oC 3 h	C1	-0.36	167.0	111.1	0.67
	C2	-0.37	154.5	110.4	0.72
	C3	-0.38	148.1	101.3	0.68
190^{o}C 2h +300 ^{o}C 2 h	C1	-0.31	125.5	85.1	0.68
	C2	-0.33	125.7	93.2	0.74
	C3	-0.34	129.7	96.8	0.75
190^{o}C 2h +350 ^{o}C 2 h	C1	-0.30	--	--	--
	C2	-0.30	104.0	83.3	0.80
	C3	-0.31	104.4	84.8	0.81

Interestingly, the feature of multiple anodic peaks reported in other studies of mesoporous TOFs [13] was also observed in our results (Fig. 4(a-c)), which is especially prominent for the sample heated at 250 ^{o}C (Fig. 4(a)). The dominant peak appears at -0.36 V and another small peak appears at about -0.07 V. Instead of being induced by the electrochemical cycling [13], such features appear in the first cycle, indicating the multifarious hydrogen injection sites available in the TOFs walls [22], and are indicative of the high surface area and porosity possessed by the novel PTA derived TOFs in this work. In the samples heated to 250 ^{o}C, these secondary peaks were diminished after a second cycle and nearly disappeared after three cycles, indicating the modification of mesostructures during this electrochemical cycling. However, this phenomenon is not apparent for samples with more stable structures achieved by heating at higher temperatures (Fig. 4(b) and (c)).

Electrochemical characteristics for such films shown in Fig. 4(a-c) were listed in Table 1. It can be seen from this table that Q^{+}/Q^{-} increased from a maximum of 0.72 for the 250 ^{o}C heated film to 0.75 for 300 ^{o}C and further to 0.81 for 350 ^{o}C heated film, indicating the improved reversibility with the heat treatment at higher temperatures. Additionally, the amount of charge (protons) that can be inserted and then extracted from the WO_3 frameworks decreased with increasing heating temperatures, suggesting a decrease in the active sites in the WO_3 frameworks. More extended CV testing showed the voltammograms started to lose resolution, after a 6th cycle for films heat treated at 300 ^{o}C, while films heat-treated at 350 ^{o}C showed stable voltammograms after 10 cycles. Such observations are in good agreement with previously reported results [13].

One of the most interesting results observed in this work is the transformation of mesostructures caused by the CV measurements. This has previously been suggested as being a possible mechanism for the evolution of the cyclic voltammograms by other workers [13], but no direct evidence has been shown. Thanks to the ordering of mesopores in the TOFs developed in this work, the XRD results shown in Fig. 4(d-f) provide clear evidences of change in the mesostructure during electrochemical cycling.

In these figures, the sample heated at the lower temperature of 250 ^{o}C for 3 h experiences more distinct changes in the mesostructures (Fig. 4(d), patterns 1-3). A distinct double peak feature is clearly seen after three cycle scans (Fig. 4(d), pattern 2). For samples previously heat treated at higher temperatures, only shifts in peak position after 3 cycles CV measurements (from 3.8 ^{o} to 3.5 ^{o}) were observed for samples previously heated to 300 ^{o}C (Fig. 4(e)), whilst the XRD pattern was nearly unchanged for samples which had been heated to 350 ^{o}C (Fig. 4(f)). These observations can be explained by the more stable framework walls resulting from the thermal treatment at higher temperatures and are consistent with CV results shown in Fig. 4(a-c). In the case of the sample heated at 300 ^{o}C for 2 h, a 2nd lower angle XRD peak becomes discernable after 7 cycles of CV tests as shown in Fig. 4(e) (pattern 3). These transformations in the structures for TOFs heated at 250 and 300 ^{o}C were confirmed to result from the electrochemical reactions occurring during CV tests as no such transformation (Fig. 4(d), patterns 0 and 0') was observable from the TOFs on the non-conductive side of the ITO coated glass, which received identical chemical and thermal treatment but did not undergo electrochemical cycling.

These modifications to the mesostructure are believed to result from expansion effects by the insertion of protons into the framework walls during reductive scans. These changes appear to be essentially

reversible because the original structure can be to a large extent restored by a post heat treatment at 100 ^{o}C for 1 h after electrochemical testing as can be seen from Fig. 4(d), pattern 4.

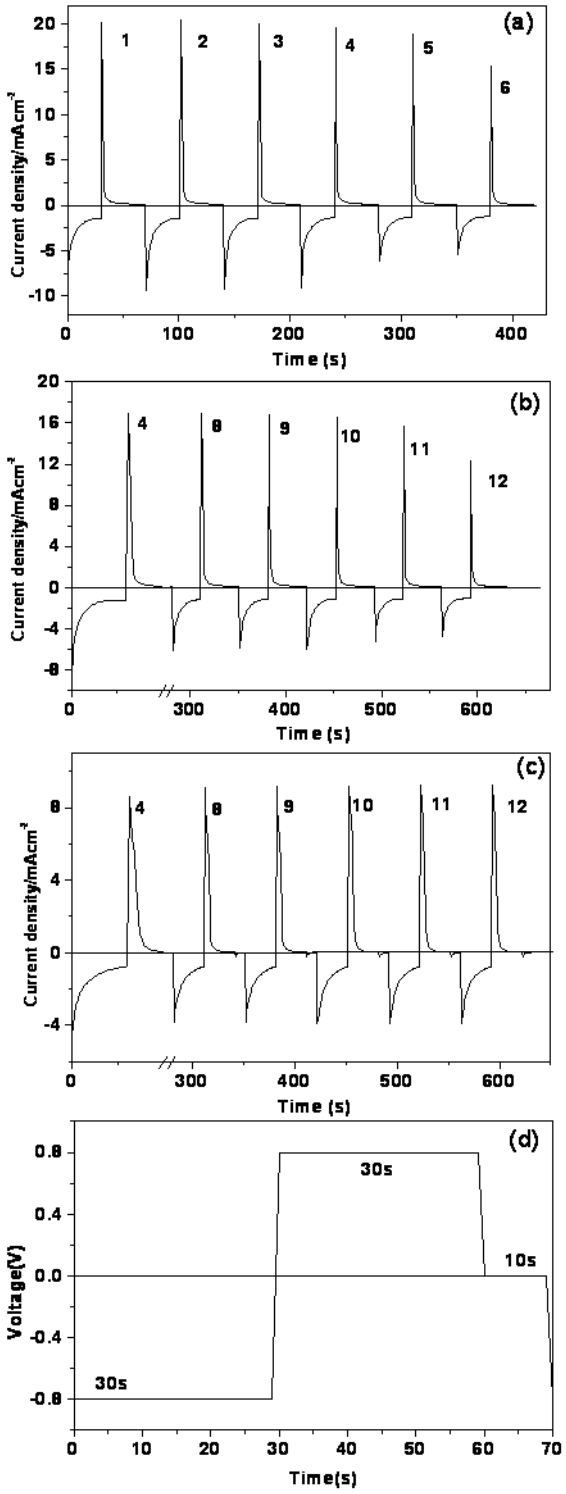

Fig. 5 Chronoamperometry measurements of mesoporous TOFs heated at (a) 250 ^{o}C 3 h (1-6 cycles), (b) 190 ^{o}C 2 h+ 300 ^{o}C 2 h (4-12 cycles), (c) 190 ^{o}C 2 h+ 350 ^{o}C 2 h (4-12 cycles), and (d) Voltage vs time curve in each cycle.

There appears to be a correlation between the changes in mesostructure as suggested by the changes in XRD patterns during electrochemical cycling in Fig. 4(d)-(f) and the changes in the corresponding CV

results in Fig. 4(a-c), providing some evidences that the structural changes described above might be responsible for the evolutions observed in the cyclic voltammograms. However, further work is required to confirm this.

Electrochemical/electrochromic properties of films heated at different temperatures were further studied in chronoamperometry measurements. The current was recorded against the voltage steps in repeating cycles (Fig. 5(d)). As can be seen from Fig. 5(a-c), there is excellent reproducibility in the initial cycles, but with differences in terms of current density emerging as the cycling proceeded depending on the previous heat treatment conditions. For samples heated at 250 ^{o}C, the current density decreased remarkably from the 5th cycle, while current density for the sample heated at 300 ^{o}C started to decrease after 9 cycles. The current densities for the sample heated 350 ^{o}C remained stable for at least 12 cycles (the test was terminated at this point). These results appear consistent with the CV results, and it is reasonable to infer that the same mechanism is responsible.

Of the variously thermally treatments used, the films heated at 250 ^{o}C showed the fastest colouration and bleaching rate of the various samples at voltage step of ±0.8 V(Fig. 5(d)), which can be seen from the extremely steep peaks (Fig. 5(a)). In comparison, among films heated at different temperatures studied in this work, the film heated at 300 ^{o}C shows slightly slower but still quite comparable colouration and bleaching rate (Fig. 5(b)); whilst the 350 ^{o}C heated film showed a significant broadening and lowering of the peaks (Fig. 5(c)), indicating a slower response.

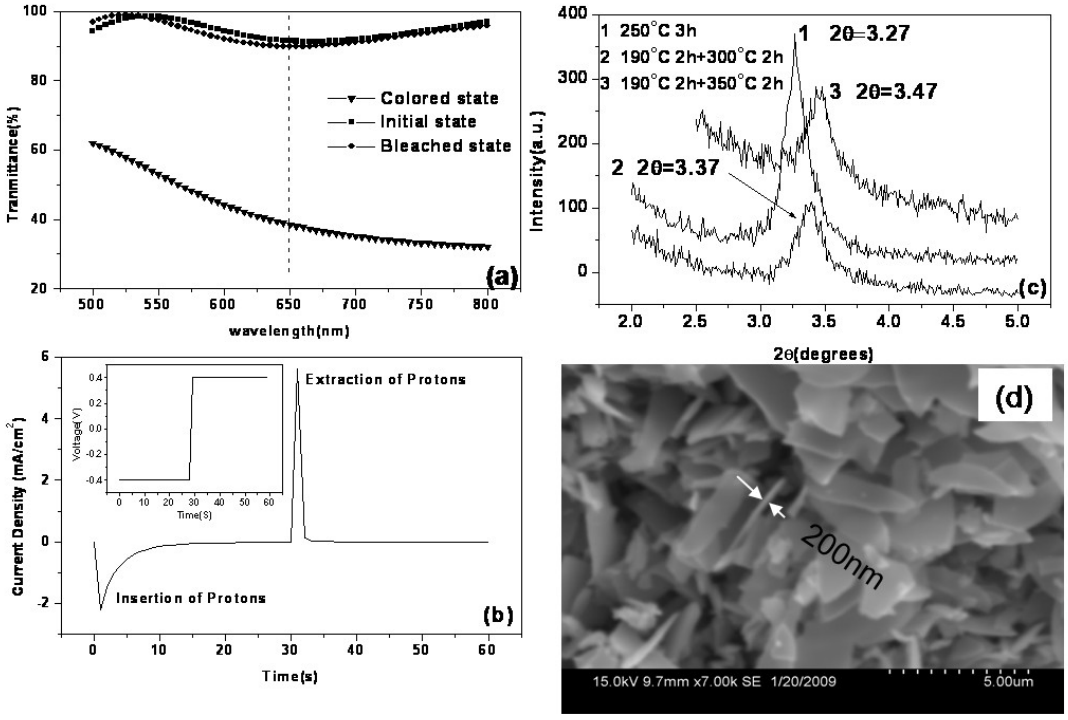

Fig. 6 (a) Optical transmittance spectra for mesoporous TOFs heated at 350 ℃, (b) Chronoamperometry measurement (8th cycles) in voltage steps between -0.4 V and 0.4 V (vs Ag) (shown inset), (c) XRD patterns of mesoporous TOFs with reduced film thickness, and (d) SEM of mesoporous TOFs (TWO coatings for more discernable) scratched from the substrate.

Table 2 Colouration efficiency and colouration/bleaching time of mesoporous TOFs heated at different temperatures.

Samples	Colouration efficiency [a] (CE)/cm^2C^{-1}			Coloration time[b](s) /Bleaching time[c](s)	Charge density [d] (mC/cm^2)
	1st cycle	4th cycle	8th cycle		
250 ℃ 3 h	65	41	47	8/10	5.1
190 ℃ 2h +300℃ 2h	34	52	44	10/2	6.9
190 ℃ 2 h +350℃ 2 h	28	49	46	11/2	8.2

a: calculated using the optical transmittance value at 650 nm.

b: Time to achieve 90% of total proton insertion capacity in 8th cycle.

c: Time to achieve 90% of total proton extraction capacity in 8th cycle.

d: based on the protons inserted into the TOFs structures within 30s under conditions specified in fig. 6.

These results provide further evidence that, under test conditions specified in Fig. 4-5, the numbers of proton injection sites are dependent on the heat treatment temperature used to prepare the films: the higher the heating temperature, the lower the number of active proton injection sites. However, this phenomenon could be also associated with the deterioration in the mesostructures resulting from the heat treatment at higher temperatures and/or the initiation of crystallization of WO_3 species in the frameworks, as it has been reported that crystalline tungsten oxide exhibits inferior kinetic performance than its amorphous counterpart [23, 24].

The most relevant parameter describing the performance of electrochromic TOFs is the colouration efficiency (CE), which is defined by:

$$CE = \frac{\Delta(OD)}{Q} = \frac{1}{Q} \times \log\left(\frac{T_b}{T_c}\right) = \frac{A_b - A_c}{Q} \qquad \text{(Eq.2)}$$

where, Δ(OD) is the variation in optical density, Q is the charge density (C/cm^2), T_b, T_c and A_b, A_c are the transmittance (T) and absorbance (A) in the bleached, coloured states, respectively. In this work, mesoporous TOFs with thickness of 100nm (Fig. 6(d) show good transparency after thermal treatment at temperatures ranging from 250 °C to 350 °C. A representative optical spectrum of such a film is shown in Fig. 6(a). The obtained mesostructures in these samples were confirmed by XRD (Fig. 6(c)), and the detailed coloration efficiencies and charge densities were summarised in Table 2.

It can be seen from Table 2 that colouration efficiencies for these TOFs stabilised at about 45 cm^2C^{-1}. Significantly, the colouration efficiency of TOFs heated at 300 °C nearly doubles the value reported on mesoporous TOFs (23.5 cm^2C^{-1} for 300 °C heated film) in ref [13] and approaches the top of the typical range (30-50 cm^2C^{-1}) of values normally reported for tungsten oxide films [25]. Additionally, compared with WCl_6-derived mesoporous TOFs reported in ref [13], the films heated at 300 °C and 350 °C showed very fast bleaching speed (<2 s), as can be seen from Fig. 6(b) and Table 2. Such performance is also superior to lamellar phase mesoporous tungsten oxide tested under similar conditions [7b], in

which time of 5 s was taken to extract majority of the inserted protons.

The highest charge density for films after heating at 350°C is up to 8.2mC/cm^2. Considering the porosity and thin film thickness (around 100nm), such a high charge density can only be explained by the high surface area arising from the small pore size and thin pore walls. By comparison, upon coloration at -0.8V (vs SCE) for 30s, the transmission at 650 nm is still as high as 29% for WCl_6 derived mesostructured TOFs with thickness over 400nm [13], whilst the transmittance at 650nm of our 350nm thick TOFs is lower than 8% when coloured at -0.4 V for 30 s. This means such TOFs have great potential in applications demanding high light-intensity modulation, and that shorter colouration time or lower over potential needed to achieve the same transmittance.

Such improved electrochromic properties arise from the well formed mesoporous structures obtained by Brij 56 templated sol-gel route from tungstic acid. More tests are under way to investigate the electrochromic stability and in organic electrolyte systems, e.g. $LiClO_4$ in propylene carbonate.

4. Conclusion

A low cost, facile sol-gel process employing tungstic acid precursor and Brij 56 surfactant templating has been developed to produce mesostructured tungsten oxide films. Hexagonally ordered mesostructures with pore size of 2-3 nm and wall thickness can be obtained after heat treatment at 400°C. Accessible mesopores formed at the surface were confirmed by TEM results.

The formation of stable mesostructures and electrochromic behaviour of resulting TOFs are proved to be dependent on the preparation conditions used, notably the heat treatment conditions, to deposit the film and remove the surfactant. In the heat treatment temperature range between 250 °C and 350 °C, the response time of coloration/bleaching increases with temperature, whilst the colouration efficiencies are essentially independent of heat treatment temperatures and the associated changes in mesostructures. Attractive electrochromic properties including fast colouration and bleaching response (10 s and 2 s, respectively) and greatly improved colouration efficiency (>44cm^{2}C^{-1}) can be obtained on such TOFs. These represent greatly improved electrochromic properties compared with those reported for other surfactant templated mesoporous tungsten oxide based films [7b, 13]. High charge density up to 8.2mC/cm^2 can be achieved on such thin (100nm) mesostructured TOFs. It is therefore believed that such TOFs have great potential in electrochromic devices.

XRD studies of the material as a function of electrochemical cycling provide what we believe to be the direct evidence of the process of mesostructural evolution in tungsten oxide materials during electrochemical cycling, which has been postulated by other workers.

References:

[1] Monk PMS, Mortimer RJ, Rosseinsky DR (2007) Electrochromism and Electrochromic Devices, Cambridge University Press, Cambridge.

[2] (a) Granqvist CG (2000) Sol Energy Mater Sol Cells 60:201; (b) Livage J, Ganguli D (2001) Sol Energy Mater Sol Cells 68:365; (c) Patra A, Auddy K, Ganguli D, Livage J, Biswas PK (2004) Mater Lett 58:1059.

[3] (a) Munro B, Kramer S, Zapp P, Drug H (1998) J Sol–Gel Sci Technol 13:673; (b) Zhuang L, Xu X, Shen H, (2003) Surf Coat Technol 167:217; (c) Leftheriotis G, Papaefthimiou S, Yianoulis P, Siokou A, Kefalas D (2003) Appl Surf Sci 218:275; (d) Deepa M, Sharma R, Basu A, Agnihotry SA (2005) Electrochim Acta 50:3545.

[4] Rougier A, Portemer F, Quédé A, EI Marssi M, (1999) Appl Surf Sci 153:1.

[5] Dipaola A, Diquarto F, Sunseri C (1978) J Electrochem Soc 125:1344.

[6] Faughnan BW, Crandall RS, Heyman PM (1975) RCA Rev 36:177.

[7] (a) Baeck SH, Jaramillo T, Stucky GD, McFarland EW (2002) Nano Lett 2:831; (b) Baeck SH, Choi KS, Jaramillo TF, Stucky GD, McFarland EW (2003) Adv Mater 15:1269; (c) Baeck SH, Jaramillo TF, Brandli C, McFarland EW (2002) J Comb Chem 4:563; (d) Meulenkamp EA (1997) J Electrochem 144:1664; (e) Yang B, Li HJ, Blackford M, Luca V (2006) Curr Appl Phys 6:436; (f) Cantalini C, Pelino M, Sun HT, Faccio M, Santucci S, Lozzi L, Passacantando M (1996) Sensors Actuators B 35-36:112.

[8] (a) Kresge CT, Leonowicz ME, Roth WJ, Vartuli JC, Beck JS (1992) Nature 359:710; (b) Beck JS, Vartuli JC, Roth WJ, Leonowicz ME, Kresge CT, Schmitt KD, Chu CTW, Olson DH, Sheppard EW, McCullen SB, Higgins JB, Schlenkert JL (1992) J Am Chem Soc 114:10834.

[9] (a) Wang W, Song M (2005) Mater Res Bull 40:1737; (b) Wang W, Song M (2006) Mater Res Bull 41:436.

[10] (a) Yang P, Zhao D, Margolese DI, Chmelka BF, Stucky GD (1999) Chem Mater 11:2813; (b) Yang P, Zhao D, Margolese DI, Chmelka BF, Stucky GD (1998) Nature 396:152.

[11] Deepa M, Srivastava AK, Sood KN, Agnihotrym SA (2006) Nanotechnology 17: 2625.

[12] Deepa M, Srivastava AK, Sharma SN, Govind and Shivaprasad SM (2008) Appl Surf Sci 254:2342.

[13] Cheng W, Baudrin E, Dunn B, Zink JI (2001) J Mater Chem 11:92.

[14] (a) Lai WH, Shieh J, Teoh LG, Hung IM, Liao CS, Hon MH (2005) J Alloy Compd 396:295; (b) Lai WH，Teoh LG, Su YH, Shieh J, Hon MH (2007) J Am Ceram Soc 90:4073; (c) Ozkan E, Lee SH, Liu P, Tracy CE, Tepehan FZ, Pitts JR, Deb SK (2002) Solid State Ionics, 149:139; (d) Sallard S, Brezesinski T, Smarsly BM (2007) J Phys Chem C 111:7200; (e) Brezesinski T, Rohlfing DF, Sallard S, Antonietti M, Smarsly BM (2006) Small 2 :1203; (f) Zayim EO, Liu P, Lee SH, Tracy CE, Turner JA, Pitts JR, Deb SK (2003) Solid State Ionics, 165:65.

[15] (a) Gesheva KA, Ivanova T, Hamelmann F (2006) Sol Energy Mater Sol Cells 90:2532; (b) Livage J, Guzman G (1996) Solid State Ionics 84 :205.

[16] Qi ZM, Zhou HS, Watanabe T, Honma I (2004) J Mater Chem 14:3540.

[17] Wang W, Pang YX, Hodgson SNB, Micro Meso Mater (2009) 121:121

[18] (a) Bagshaw SA, Prouzet E, Pinnavaia TJ (1995) Science 269:1242; (b) Bagshaw SA, Pinnavaia TJ (1996) Angew Chem., Int Ed Engl 35:1102

[19] (a) Kim S, Pauly TR, Pinnavaia TJ (2000) Chem Commun 935; (b) Lei J, Liu D, Guo L, Yan X, Tong H (2006) J Sol-Gel Sci Technol 39:169

[20] Yuan JG, Zhang YZ, Le J, Song LX, Hu XF (2007) Mater Lett 61:1114.

[21] (a) Deepa M, Singh P, Sharma SN, Agnihotry SA (2006) Sol Energy Mater Sol Cells 90:2665; (b) Deepa M, Sharma N, Varshney P, Agnihotry S.A (2000) J Mat Sci 35:5313.

[22] Kim DJ, Pyun SI, (1997) Solid State Ionics 99:185.

[23] Antonaia A, Addonizio ML, Minarini C, Polichetti T, V-Antisari M (2001) Electrochim Acta 46:2221.

[24] Antonaia A, Polichetti T, Addonizio M L, Aprea S, Mi-narini C, Rubino A (1999) Thin Solid Films 354:73.

[25] Granqvist CG (2002) Handbook of Inorganic Electrochromic Materials; Elsevier: Amsterdam.